

Wetting behavior and interfacial microstructure of palladium- and silver-based braze alloys with C–C and SiC–SiC composites

Rajiv Asthana · Mrityunjay Singh ·
Natalia Sobczak

Received: 18 November 2009 / Accepted: 21 May 2010 / Published online: 8 June 2010
© Springer Science+Business Media, LLC 2010

Abstract High-temperature sessile-drop wettability tests were conducted on unpolished C–C and SiC–SiC composite substrates using commercial braze alloys Palco (Pd-35Co), Palni (Pd-40Ni), Cusil-ABA (63Ag-35.3Cu-1.75Ti), and Ticusil (68.8Ag-26.7Cu-4.5Ti). Observations revealed non-uniform, anisotropic spreading, copious braze infiltration of the composite substrates, particularly C–C composite, and Ti enrichment at the composite/braze interface together with dissolution of Si (from SiC–SiC composite) in braze and diffusion of Co (from Palco) in the composite. The droplet/composite contact region near the droplet center revealed intimate and microstructurally sound bonding. However, inter-laminar shear cracking within the SiC–SiC composite in contact with Ticusil, Palco, and Palni, and partial substrate/droplet de-cohesion near the edge of the droplet were also observed. In Palco and Palni droplets, fiber tows in the contact region de-laminated from the main body of the composite via inter-laminar shear cracking resulting in fiber flotation, segregation, and surface degradation. The study is one of the first empirical enquiries into the complex wetting and spreading behavior of brazes on commercial C–C and SiC–SiC composites.

Introduction

Carbon–carbon, silicon carbide–silicon carbide, and carbon–silicon carbide composites have been developed and tested under severe operating conditions for demanding aerospace and ground-based applications. Although these composites offer higher toughness than monolithic ceramics, their net-shape manufacture into complex shapes via conventional ceramic forming and machining is usually quite difficult. Joining and integration technologies enable hierarchical design and manufacturing of intricate ceramic-matrix composite (CMC) parts starting with geometrically simpler units that are subsequently joined to themselves and/or to metals to create components with progressively higher levels of complexity and functionality. Robust joining technology such as brazing, diffusion bonding, and adhesive bonding can, therefore, play a critical enabling role in the development and deployment of such composites. Active metal brazing, in particular, is simple and cost-effective alternative to more elaborate joining procedures and has been used to join CMCs [1–13] such as ZrB₂-based ultra-high-temperature ceramic composites [5–7], C–C [8–12], and C–SiC and SiC–SiC [13]. Braze alloys usually contain a reactive filler metal (e.g., Ti, Cr, V, Hf, etc.) that promotes braze wettability and spreading by inducing chemical reactions with the ceramic.

Extensive studies have been done on the wettability of monolithic ceramics, carbon, and select CMCs. Klein et al. [14] studied the wettability of hot-pressed fully dense Si₃N₄-matrix composites containing at least 27% TiN, TiB₂, HfB₂, or MoSi₂ by Cu–Ag and Cu–Ag–Ti alloys. Non-wetting was observed with Ag, Cu and Ag–Cu alloy on all composites but the addition of 3 wt% Ti to Ag–Cu alloy-induced reaction and wetting. Similarly, sessile-drop wetting tests on HIP AlN–TiB₂ ceramic composites by Cu,

R. Asthana (✉)

Department of Engineering & Technology, University
of Wisconsin-Stout, Menomonie, WI 54751, USA
e-mail: asthanar@uwstout.edu

M. Singh

Ohio Aerospace Institute, NASA Glenn Research Center,
Cleveland, OH 44135, USA

N. Sobczak

Center for High-Temperature Studies, Foundry Research
Institute, 30-418 Krakow, Poland

Ag and Cu–Ag alloys showed a non-wetting behavior [15]; however, wetting occurred for CuAgTi brazing alloys and for pure Ni, which diffused into the ceramic. Passerone and coworkers [1] investigated the wetting and joining behaviors of Al₂O₃–ZrO₂ composites by AgCuTi braze and observed a contact angle of 22°. The metal/composite interface had irregular morphology and revealed liquid penetration with preferential wetting of the zirconia grains many of which were engulfed into the metallic alloy. These studies provide useful scientific data and highlight the complexity of the high-temperature capillarity phenomena in chemically inhomogeneous multiphase ceramics. There is scant information on the wettability and spreading of commercial braze alloys on C–C and SiC–SiC composites at high temperatures. Characterizing braze wettability and spreading on such substrates not only represents a research opportunity for scientific investigation but also a critical need for the practitioner engaged in joining of CMCs.

In this article, the droplet spreading behavior and interface microstructure of two commercial Pd-base brazes, Palco (Pd-35Co) and Palni (Pd-40Ni), and two AgCuTi brazes, Cusil-ABA (63Ag–35.3Cu–1.75Ti) and Ticusil (68.8Ag–26.7Cu–4.5Ti), on C–C and SiC–SiC composites have been investigated. The sessile-drop wettability tests were conducted on as-received (unpolished) composite substrates to simulate the actual joining conditions, and the joint interfaces in solidified sessile-drop couples were examined using optical and scanning electron microscopy coupled with energy dispersive spectroscopy. The study presumably is one of the first attempts to empirically evaluate the complex spreading behavior of select braze alloys on commercial C–C and SiC–SiC composites.

Experimental procedure

The 3-D C–C composites with a CVI carbon matrix from Goodrich Corp., Santa Fe, CA, USA, and SiC–SiC composites containing Sylramic SiC fiber in a melt-infiltrated (MI) SiC matrix from GE Power System Composites, DE,

USA, were used as substrates. The finished slurry cast MI SiC–SiC composites nominally contain 35 vol% fiber, 6 vol% fiber coating, 25 vol% CVD SiC, 16 vol% SiC particulate from the slurry, 12 vol% Si alloy, and 6 vol% porosity. Most of the porosity is a result of the “canning” of the fiber tows during the CVI steps, which makes it inaccessible to slurry and molten Si in the later steps of the fabrication process.

The sessile drop tests were conducted on as-received composite substrates (i.e., freshly cut but unpolished substrates in order to avoid introducing the polishing material into the substrate surface). The braze foils (~25 μm thick) of Cusil-ABA, Ticusil, Palco and Palni, from Morgan Advanced Ceramics, Hayward, CA, with the physical and mechanical properties listed in Table 1, were used in the sessile drop wetting tests. The substrates and braze foils were ultrasonically cleaned in acetone prior to the wetting tests. The braze foil was manually rolled and placed on the substrate with the circular edge of the rolled foil in contact with the substrate. Practically all of the wettability tests were done using contact heating (CH) of substrate/braze couples under 10⁻⁶–10⁻⁵ mbar vacuum for 5 min contact; this relatively short time of contact was used for consistency with brazing practice although it also presumably led to measurement of transient, not equilibrium, contact angles. Additionally, one test on SiC–SiC composite with Palni was done using the capillary purification (CP) technique. In the CP technique, the CMC substrate and braze were heated simultaneously but separately under vacuum, the braze in a graphite syringe. At the test temperature, a droplet of molten braze was mechanically extruded out of the graphite syringe and brought in contact with the pre-heated ceramic. The extrusion action in CP yields droplets free of surface oxides, and the separate heating eliminates chemical interactions that would occur during contact heating prior to the test. Table 2 lists the various braze/composite combinations studied. At the conclusion of the sessile-drop test, the joined specimens were prepared for metallography and examined using optical microscopy (OM) and scanning electron microscopy (SEM) coupled

Table 1 Selected physical and mechanical properties of braze alloys used in the study

Braze	T_L , K	T_S , K	E , GPa	YS, MPa	CTE, $\times 10^{-6}$ K ⁻¹	K , W/m K	%El
TiCuSil ^{®a}	1,173	1,053	85	292	18.5	219	28
Cusil-ABA ^{®a}	1,088	1,053	83	271	18.5	180	20
Palco ^{®a}	1,492	1,492	–	341	15.0 ^b	35	43
Palni ^{®a}	1,511	1,511	–	772	15.0 ^b	42	23

T_L liquidus temperature, T_S solidus temperature, E Young's modulus, YS yield strength, CTE coefficient of thermal expansion, K thermal conductivity, %El percent elongation

^a Morgan Advanced Ceramics, Hayward, CA

^b Estimated CTE [19]

Table 2 Droplet/substrate couples for the wettability test and microstructure analysis with corresponding wetting test conditions and braze contact angle on CMC

Sample ID	Braze		Composite substrate	Testing conditions	Vacuum level, mbar	Contact angle, θ	Surrounding metallic ring
	Type	Composition, wt%					
1416	Palni [®]	Pd-40Ni	MI SiC–SiC	CH, 1,315 K, 5 min	9.38×10^{-6} 1.14×10^{-5}	23°	Yes
1418	Palco [®]	Pd-35Co	MI SiC–SiC	CH, 1,392 K, 5 min	1.30×10^{-5} 1.79×10^{-5}	18–26°	No
1420	Ticusil [®]	68.8Ag–26.7Cu–4.50Ti	MI SiC–SiC	CH, 1,181 K, 5 min	1.85×10^{-6} 1.56×10^{-6}	50°	Yes
1432	Cusil-ABA [®]	63Ag–35.3Cu–1.75Ti	MI SiC–SiC	CH, 1,088 K, 5 min	1.83×10^{-6} 1.57×10^{-6}	50–73°	Yes
1449	Palco [®]	Pd-35Co	C–C	CH, 1,657 K, 5 min	1.05×10^{-5} 9.40×10^{-6}	46–50°	No
1450	Cusil-ABA [®]	63Ag–35.3Cu–1.75Ti	C–C	CH, 1,088 K, 5 min	1.33×10^{-5} 1.09×10^{-5}	35°	No
1452	Palni [®]	Pd-40Ni	C–C ^a	CH, 1,513 K, 5 min	4.04×10^{-5} 3.66×10^{-5}	47°	No
1453	Ticusil [®]	68.8Ag–26.7Cu–4.50Ti	C–C	CH, 1,073 K, 5 min	7.42×10^{-6} 6.91×10^{-6}	27°	No
1454	Cusil-ABA [®]	63Ag–35.3Cu–1.75Ti	C–C	CH, 1,073 K, 5 min	4.11×10^{-5} 3.68×10^{-5}	60°	No
1455	Palni [®]	Pd-40Ni	MI SiC–SiC	CP, 1,513 K, 5 min	7.54×10^{-5} 5.31×10^{-5}	33–87°	Yes

^a The joint failed under low mechanical load and could not be examined

with energy dispersive spectroscopy (EDS) on a JEOL 840A unit. An accelerating voltage of 20 kV was used to operate the SEM in secondary electron (SE) imaging mode.

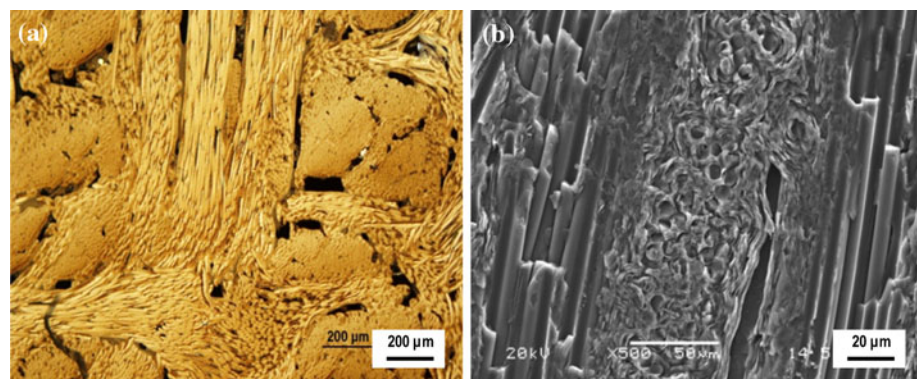
Results and discussion

Spreading behavior

Figure 1a, b shows the inhomogeneous surface morphology and surface porosity in as-received (unpolished) C–C and SiC–SiC composite substrates. The 3-D fiber architecture in

the composites leads to different fiber orientations at the contacting surface. Figure 2a, b displays the most representative top-views of spreading droplets during the CH sessile-drop tests on CMC substrates. The droplet spreading in most cases reveals strong anisotropy. Although the initial contact between the braze foil and composite substrates was circular (i.e., edge of the rolled foil was in contact with the substrates), the non-symmetrical spreading of melted droplet points to directionally non-uniform spreading. The effect is particularly pronounced for the CP test (Fig. 3) when initial droplet of perfect spherical shape was produced by squeezing the braze metal through a capillary and thus

Fig. 1 a C–C and b SiC–SiC composite surface prior to the sessile drop test



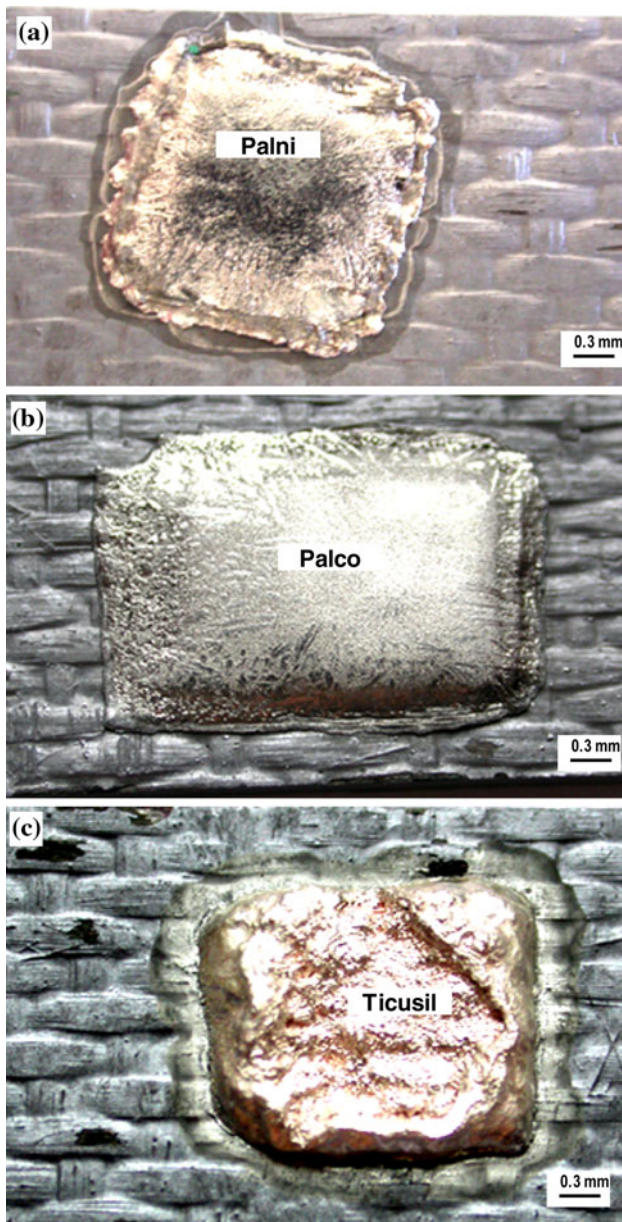


Fig. 2 Top-views of braze/SiC-SiC couples with **a** Palni (#1416: CH, 1,315 K, 5 min); **b** Palco (#1418: CH, 1,392 K, 5 min); and **c** Ticusil (#1420: CH, 1,181 K, 5 min) showing non-uniform spreading. For Palni (**a**) and Ticusil (**c**) a metallic ring (*hallo*) around the droplet is well distinguished and it corresponds to metal infiltrated region. A similar ring was observed with Cusil-ABA

there were no perturbation of the initial shape of the braze metal or its interaction with composite substrate surface during heating to the wetting test temperature. The genesis of observed anisotropic spreading could be traced either to the chemical or morphological inhomogeneity of the CMC substrates, or both. Additionally, as discussed later, copious braze infiltration had occurred in some CMC substrates; this would affect the measured contact angles because of a loss of the liquid and corresponding change in the droplet

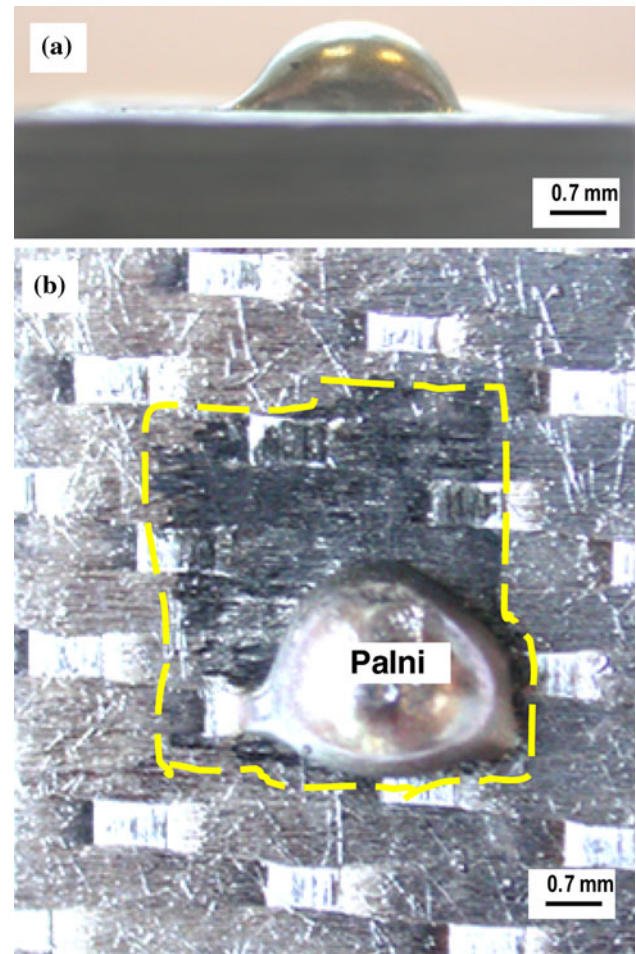
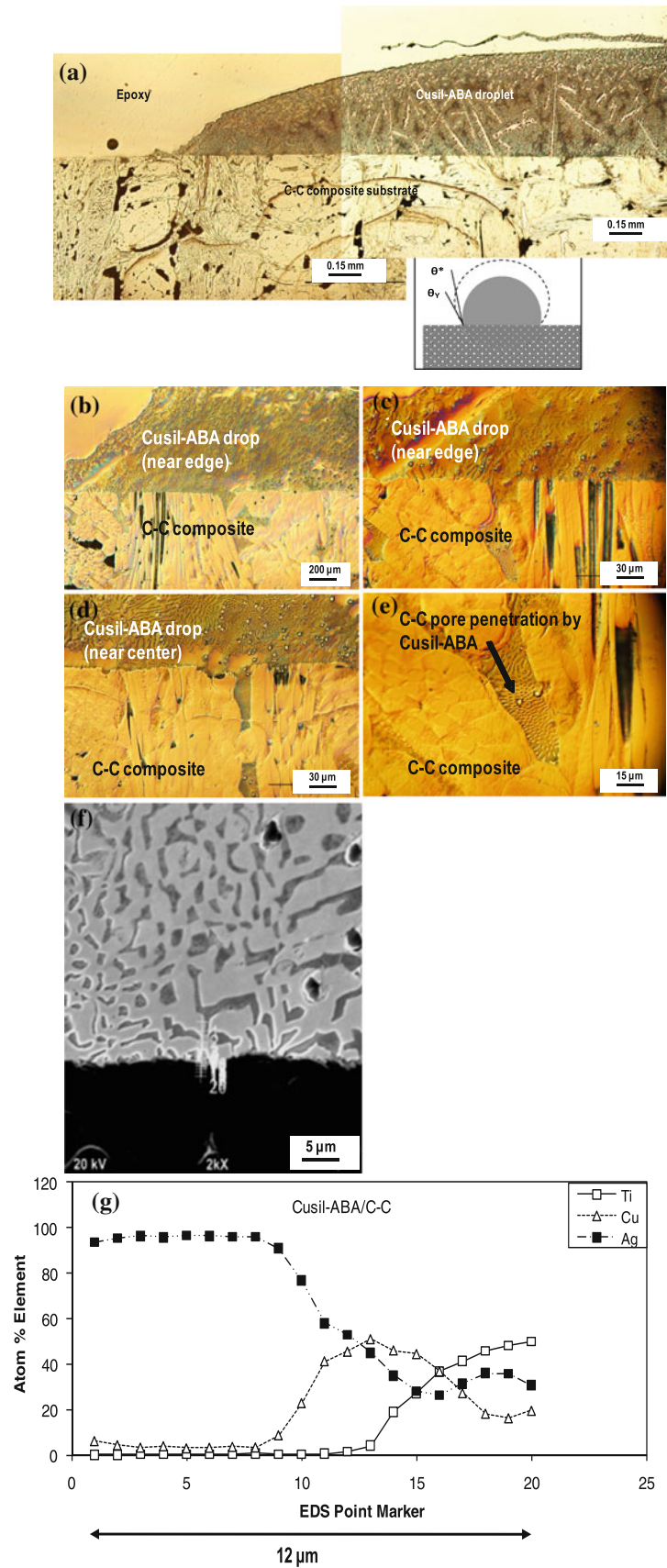


Fig. 3 **a** Side-view and **b** top-view of the Palni/SiC-SiC couple (CP, 1,513 K, 5 min) showing wetting hysteresis and nonuniform spreading affected by the fiber orientation due to physical and chemical heterogeneity of the substrate. The *dashed line* marks the area corresponding to metal infiltrated region

volume. Thus, only approximate values of the contact angle could be extracted from these sessile drop tests; these values are summarized in Table 2. The solidified droplets were visibly bonded to the substrates and could not be dislodged using manual force except in Palni/C-C couples where separation occurred readily (no further examination was done on Palni/C-C).

The wettability test results summarized in Table 2 provide some important observations. First, even at wettability test temperatures significantly (e.g., ~ 200 °C) below the manufacturer-provided braze alloy liquidus temperatures, braze foils melted and began to spread on CMC substrates (e.g., samples 1416, 1418, 1453, and 1454). There are two reasons for melting and wetting starting at $T < T_L$. First, the dissolution of substrate into the braze leads to deep eutectics (e.g., Si in PdNi), and second, the presence of a eutectic in the phase diagram of the CuAgTi braze itself.

Fig. 4 Cusil-ABA/C-C couple (# 1450, CH, 1,088 K, 5 min): **a** overall view of the droplet (inset shows schematic modulation of contact angle due to infiltration); **b, c** droplet/composite interface near the droplet periphery; **d, e** interface near the droplet center showing braze infiltration of interfiber channels; **f, g** braze/composite interface region near the droplet center and the corresponding elemental profiles across the interface



It is, therefore, conceivable that chemical diffusion and elemental dissolution during contact heating could lower the liquidus temperature of braze (e.g., small percentages of Si from SiC–SiC or proprietary constituents containing boron from sealants in C–C could dissolve in braze and lower its liquidus temperature). Table 2 shows that in all droplet/CMC couples, the contact angle values were acute with the Palco and Palni brazes exhibiting the lowest angles of 18–26° even when the wettability test temperature was appreciably below the braze liquidus temperature. Interestingly, Palni on SiC–SiC with the CP technique yielded slightly higher (33–87°) but wettable ($\theta < 90^\circ$) values of contact angle at 1,513 K as compared to the same couple with the CH technique at a significantly lower temperature of 1,315 K (e.g., CH Sample No. 1416 and CP Sample No. 1455). Conceivably, chemical interactions during contact heating of the couple lowered not only the braze liquidus but also the droplet/CMC contact angle due presumably to favorable interfacial changes that led to θ values lower than those obtained with the CP technique. There will be more extensive CMC/braze interaction in CH than CP because of longer contact in CH (especially at sub-liquidus temperatures during heating). Normally, “cleaner” oxide-free droplets obtained via CP have been known to yield lower contact angles than CH. The opposite observation of higher observed angles in CP for SiC–SiC/Palni suggests that favorable surface modification via CMC/braze reactions overrides the beneficial effects of surface oxide removal on the droplet. Indeed, for CH SiC–SiC/Palni couples, the test temperature of 1,315 K is about 87% of the absolute braze liquidus, and diffusion processes

could be rapid and extensive. Thus, although wettability shall generally improve at high temperatures, these observations suggest the feasibility of at least partial low-temperature surface modification and bonding even without having to melt the metal. Evidence abounds in the literature of surface modification at low temperatures; for example, in Ni/sapphire couples, solid Ni bonded to the sapphire even at temperatures significantly below the melting point of pure Ni [16].

Grigorenko et al. [17] studied the high-temperature wettability of NiPd alloys on SiC. At 1,523 K and 1,623 K, Ni₅₅Pd₄₄ alloy on α -SiC rapidly attained an equilibrium contact angle of 18° in 1.6 and 0.9 s, respectively [17]; the contact angle decreased exponentially with time. According to Grigorenko et al., Pd diminished the wetting of pure Ni on SiC, but the decrease in contact angle was still rapid. The initial wetting rate at 1,523 K was $\sim 2.1 \times 10^4$ deg/s and the initial spreading rate was 48 cm/s; the spreading kinetics could be fitted to the power law equation: $r = kt^n$, where r is the displacement of the wetting front from the initial contact point, t is time, and K and n are system-specific constants ($n = 0.26$ for the Ni₅₅Pd₄₄/ α -SiC at 1,523 K). The authors noted that wetting on their monolithic α -SiC substrates was controlled by a mixed chemical kinetic-inertial flow regime. It must, however, be noted that there is some uncertainty about the exact effect of Pd on the wettability of Ni on SiC. For example, according to ref. [18–20], the equilibrium contact angles of Ni on SiC are more than 36° at 1,623–1,773 K indicating that Pd alloying of Ni might actually improve the wetting (e.g., a contact angle of 18° [17] for NiPd/SiC system). Likewise, the

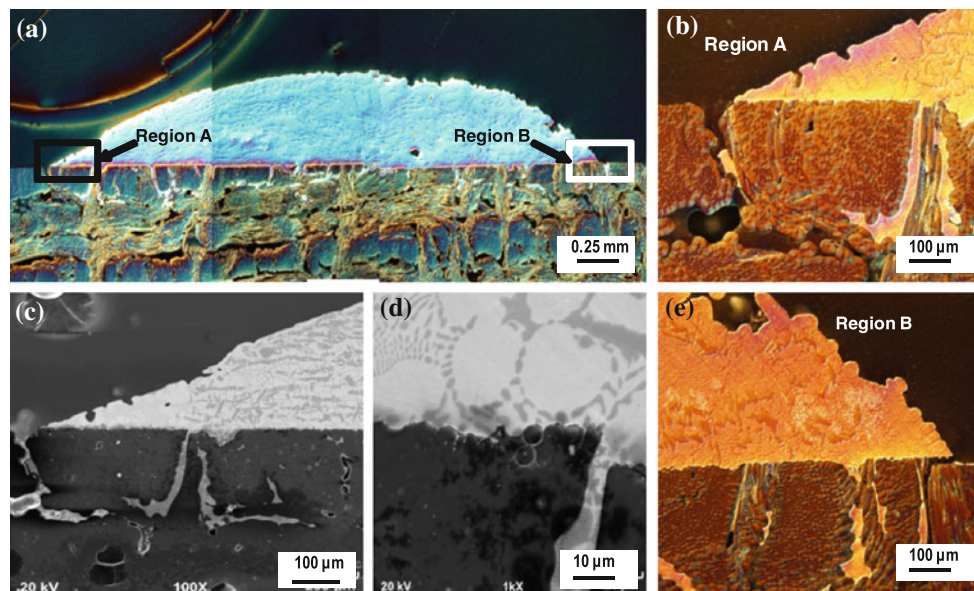
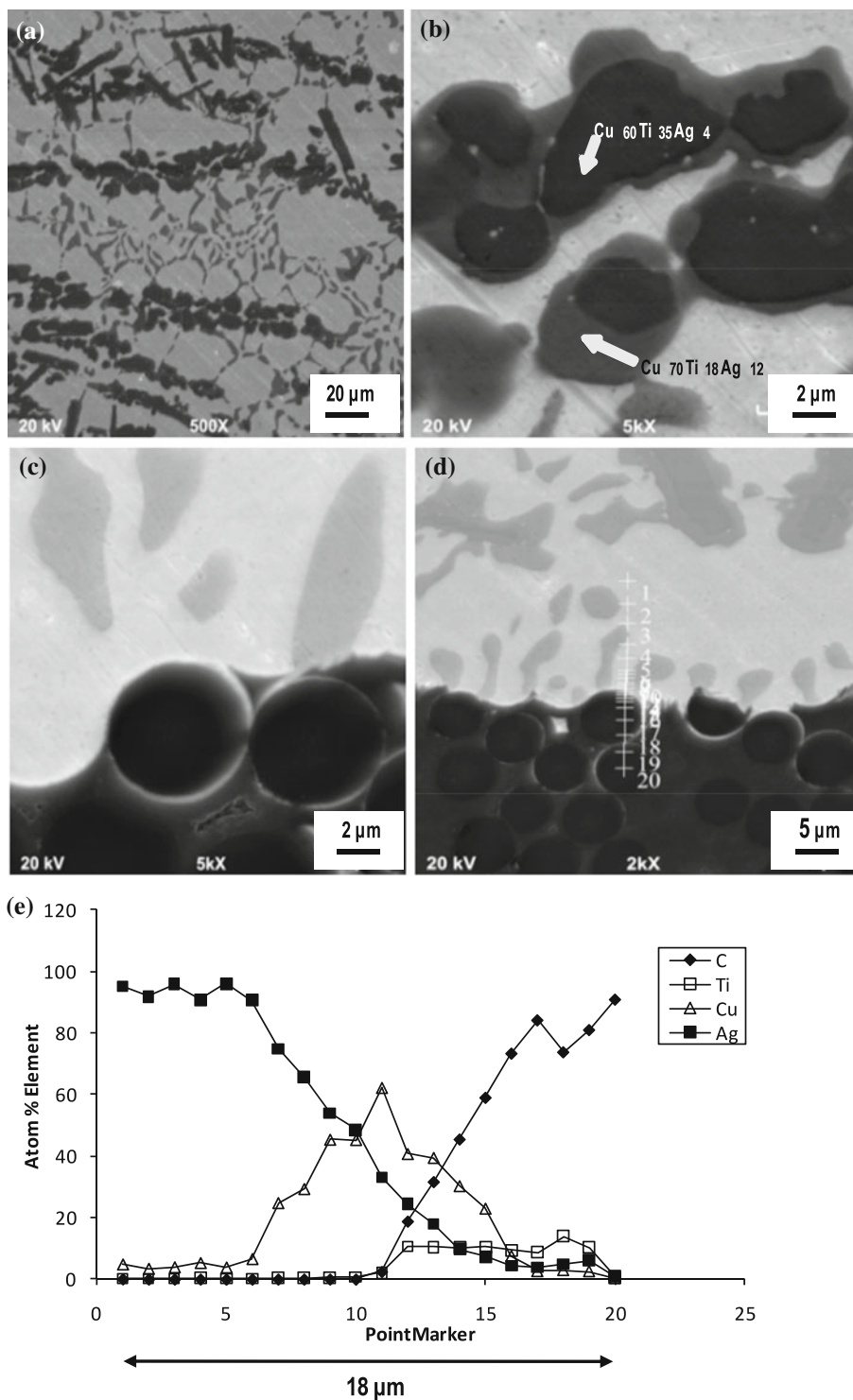


Fig. 5 Ticusil/C–C couple (#1453, CH, 1,073 K, 5 min): **a** overall view of the drop; **b**, **c** region ‘A’ of **a**, **d** joint interface near the droplet center; **e** region ‘B’ of **a**. Copious braze infiltration and substrate cracking near the droplet periphery

Fig. 6 Ticusil/C–C couple (#1453, CH, 1,073 K, 5 min): **a, b** microstructure in the droplet center, **c, d** microstructure at the composite/braze interface near the drop center, and **e** elemental distribution at point markers of **d**



equilibrium contact angle in Si/SiC system is about 30–50°; however, many equilibrium contact angle values of Me–Si/SiC systems (e.g., Au–10Si/SiC) are less than that of Si/SiC. Thus, Pd may not always diminish the wetting of pure Ni on SiC, although the addition of Pd can reduce the concentration of Ni.

The NiPd alloy composition used by Grigorenko et al. [17] is rather similar to the Palni braze composition used in this study (Pd–40Ni); however, the spreading behavior in our study was strongly influenced by surface inhomogeneity (roughness) and surface chemistry of the composite substrates. Roughness effects on wettability in

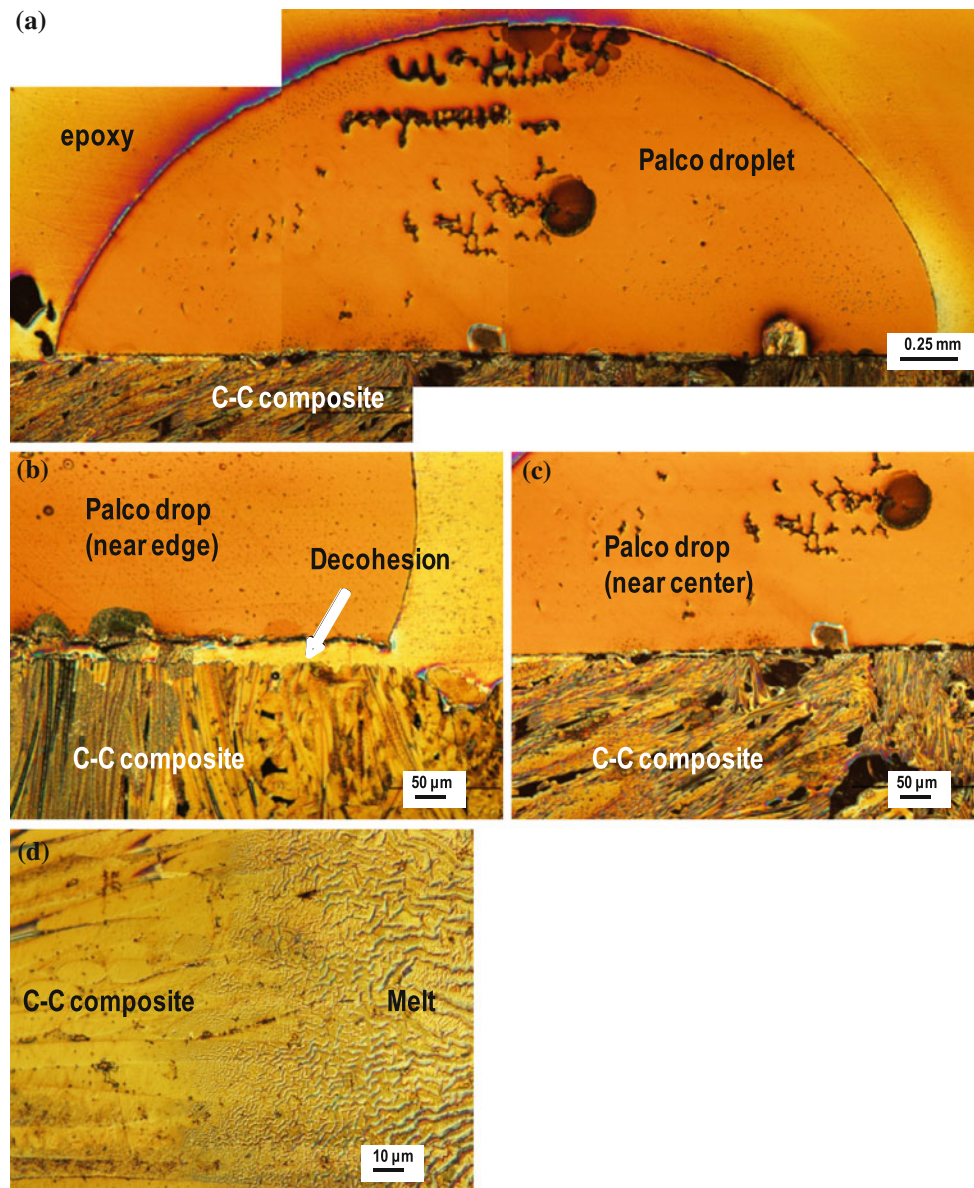
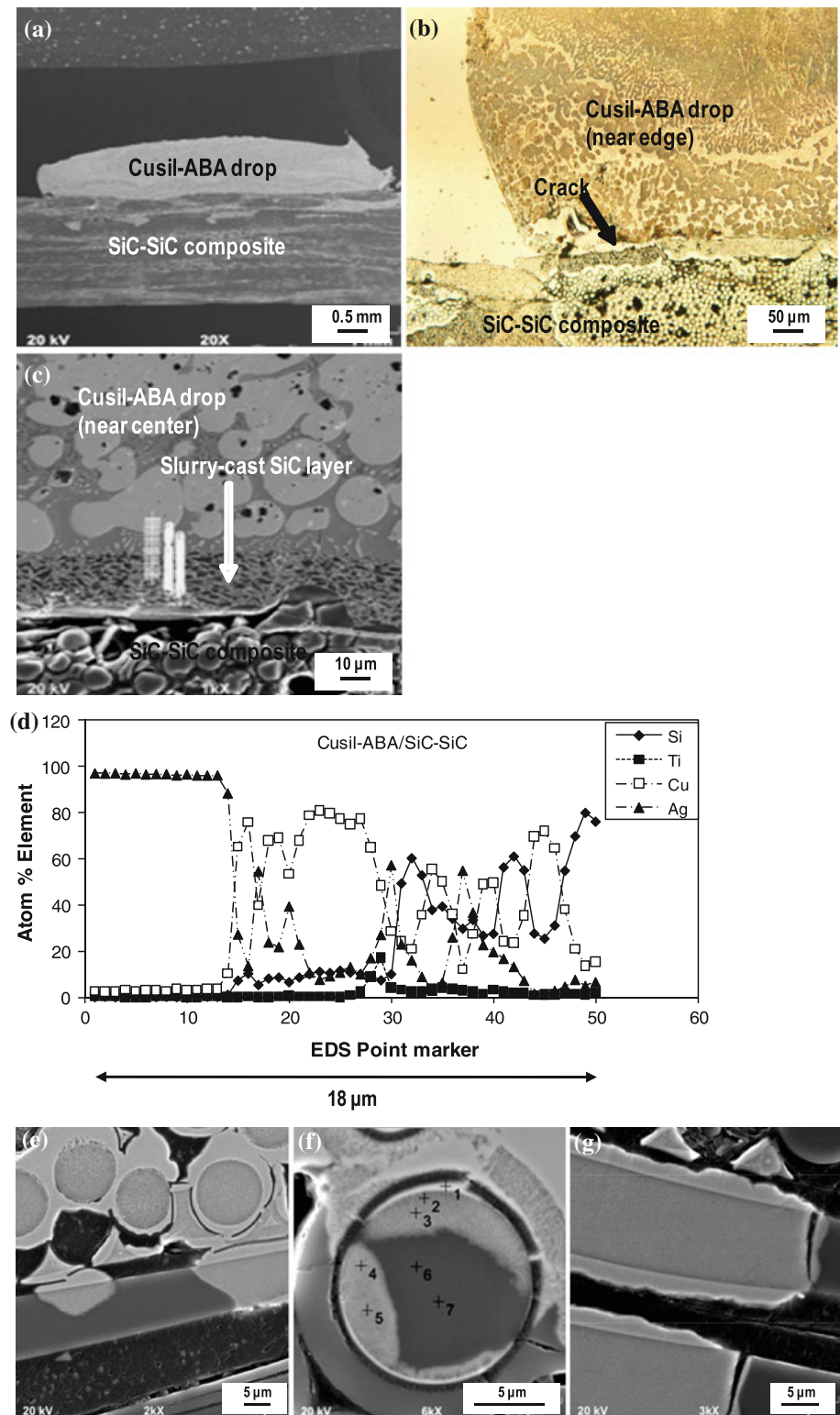


Fig. 7 Palco/C–C couple (#1449, CH, 1,657 K, 5 min): **a** overview of the droplet, **b** view near the droplet periphery showing interfacial de-cohesion, **c** contact region near the droplet center, and **d** braze spreading over the composite

low-temperature, chemically inert systems are usually described by the well-known Wenzel equation ($\cos\theta_R = W_R \cos\theta_0$, where θ_R and θ_0 are the contact angles on rough and smooth surfaces, respectively, and W_R is the roughness area ratio). For wettable systems, contact angle generally decreases with increasing roughness. Likewise, contact angles on chemically inhomogeneous surfaces are expressed by Cassie's equation in terms of the area fraction-weighted angles; this equation (cited in [21]) is: e.g., $\cos\theta_e = f_1 \cos\theta_1 + f_2 \cos\theta_2$, where θ_e is an effective angle, and f_1 and f_2 are the area fractions of chemically different regions with contact angles θ_1 and θ_2 , respectively. These equations permit reliable estimates of contact angles to be obtained on surfaces with an orderly distribution of

roughness (or chemical inhomogeneity). The SiC–SiC and C–C composite substrate surfaces, however, are chemically and structurally extremely inhomogeneous, displaying considerable variations in surface chemical make-up, roughness, porosity and fiber distribution. These factors potentially could lead not only to departure from the spreading behavior observed on monolithic SiC substrates of [17] but also render quantitative prediction of contact angles prohibitively difficult. The spreading of droplets on heterogeneous substrates containing a degree of porosity (with accompanying braze infiltration) poses considerable methodological challenges in characterizing the wettability, particularly in high-temperature systems [22, 23].

Fig. 8 Cusil-ABA/SiC–SiC couple (#1432, CH, 1,088 K, 5 min): **a** overview of the droplet; **b** droplet periphery showing interfacial cracking; **c** braze/SiC–SiC interface near drop center; **d** Si, Ti, Cu, and Ag concentrations at point markers of **c**; and **e–g** show partially wetted SiC fibers in the composite

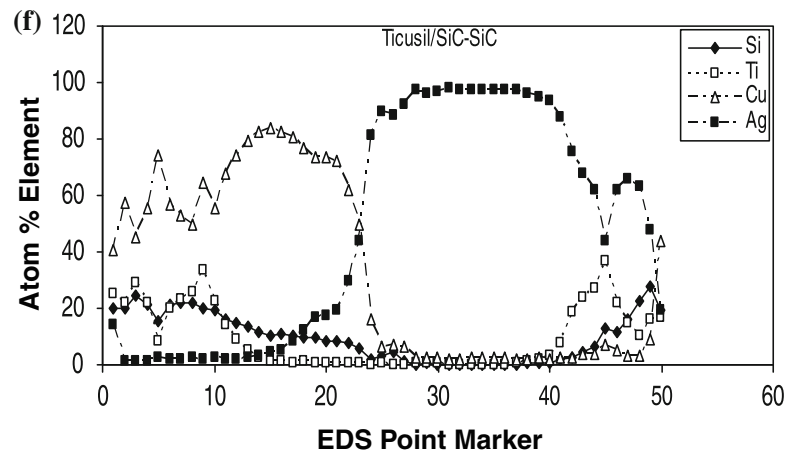
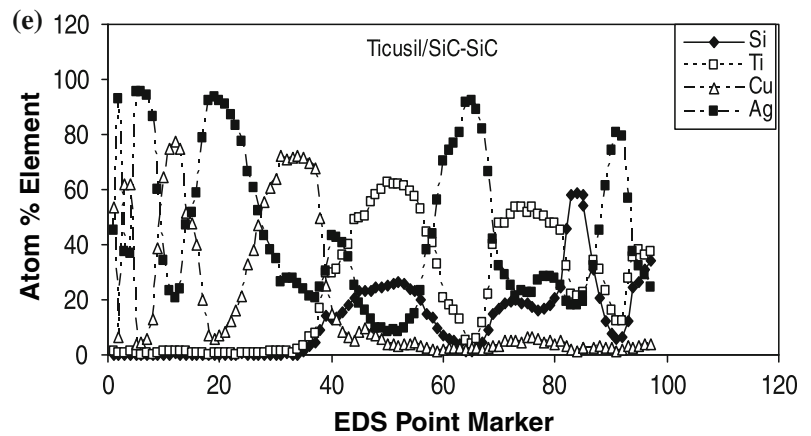
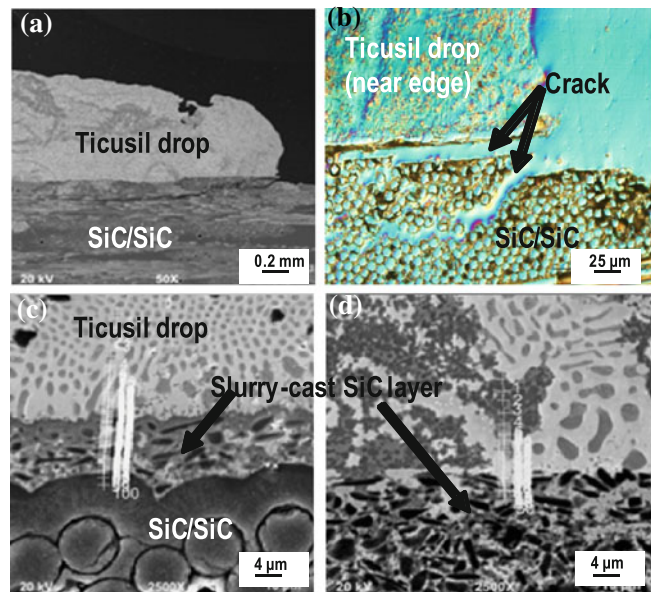


The wetting of AgCuTi brazes on carbon and monolithic SiC substrates is excellent and the equilibrium contact angles approach low acute values after short contact. For example, Ag–39Cu–3.7Ti alloy on SiC yields a contact angle of 25° in about 15 min of contact [24].

Microstructure

Because of strongly anisotropic spreading, the main focus of the study shifted toward examination of joint microstructure. Figures 4, 5, 6, 7, 8, 9, 10, 11, and 12 display the

Fig. 9 Ticusil/SiC–SiC couple (#1420, CH, 1,181 K, 5 min): **a** view of the droplet; **b** interface near the droplet edge; **c, d** interface near **c** drop edge and **d** drop center; and **e** and **f** show the elemental profiles at point markers shown in **c** and **d**, respectively

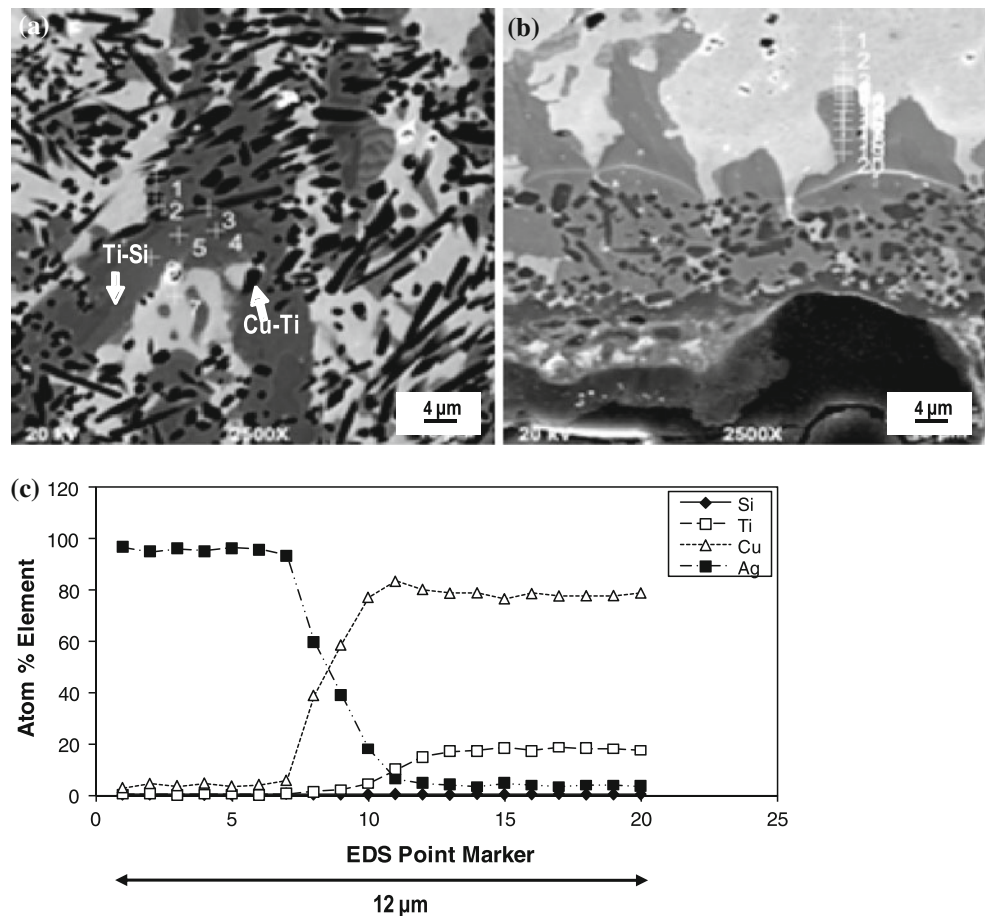


microstructure and elemental compositions of droplet/composite couples examined in this study. The Cusil-ABA/C–C couple (Fig. 4) exhibits a crack-free joint with intimate droplet/composite contact (Figs. 4a–d), copious braze infiltration of the porous composite (Fig. 4d, e), and the presence of excess titanium at the interface (Fig. 4f, g). The extensive

braze infiltration could modulate the contact angle, if measured, due to droplet volume effect. The Cusil-ABA/C–C joint is visibly devoid of bulk interfacial reaction layers. No evidence of damage to the fibers and the composite is seen.

In Ticusil/C–C couple (Fig. 5a), extensive braze infiltration (Fig. 5b–e) and substrate cracking (Fig. 5b) had

Fig. 10 Ticusil/SiC–SiC couple of Fig. 9 (#1420, CH, 1,181 K, 5 min) showing the **a** droplet microstructure near the interface, **b** interface microstructure, and **c** elemental composition at point markers of **b**. The dark plate-like particles are a Cu–Ti phase and the large light gray phase is a Ti–Si phase



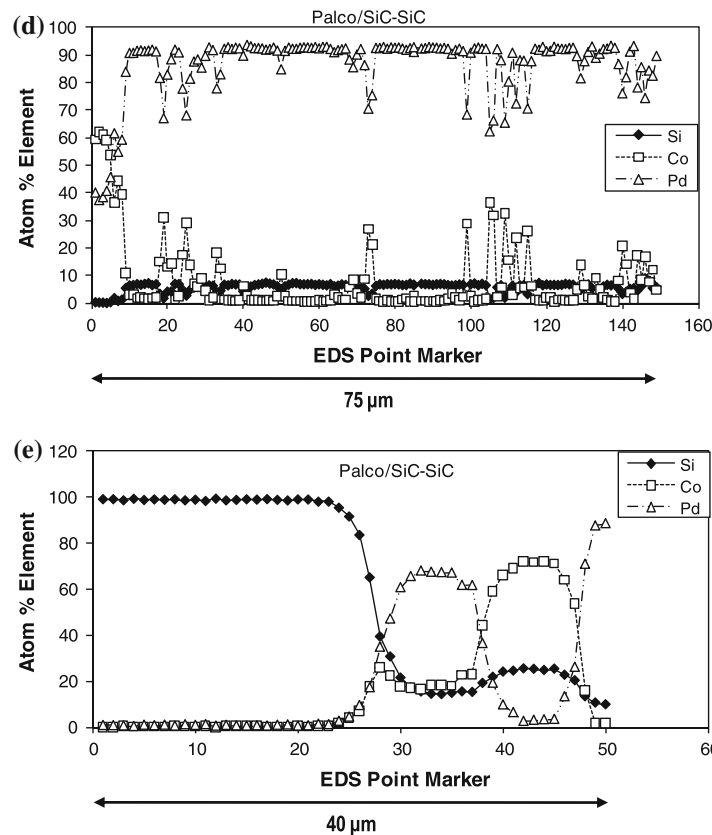
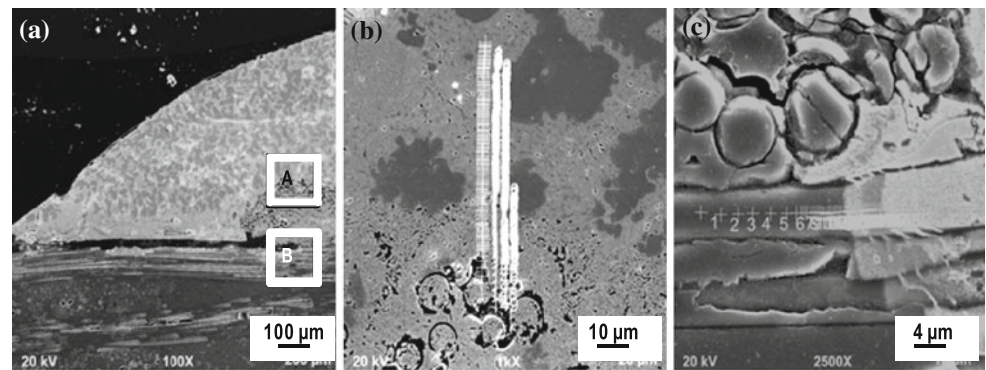
occurred whereas no cracking had occurred in Cusil-ABA/C–C joints (Fig. 4). Although Ticusil is more ductile (28% elongation, Table 1) than Cusil-ABA (20% elongation), it has higher yield strength (292 MPa) than Cusil-ABA (271 MPa) and a higher liquidus temperature ($\sim 85^\circ$ higher) than Cusil-ABA. The higher temperature could yield larger thermal strains, $\Delta\alpha\Delta T$ ($\Delta\alpha$ —CTE mismatch, ΔT —temperature interval) in Ticusil joints in comparison to Cusil-ABA joints thereby causing cracking in the Ticusil/C–C couple (Fig. 5b). The Ticusil droplet microstructure (Fig. 6a) shows Ag–Cu eutectic matrix together with CuTiAg phases (Fig. 6b) of approximate compositions (in at%): $\text{Cu}_{60}\text{Ti}_{35}\text{Ag}_4$ (dark gray platelets) and $\text{Cu}_{70}\text{Ti}_{18}\text{Ag}_{12}$ (light gray phase). The composite/braze interface (Fig. 6c, d) does not show evidence of bulk reaction layer formation. Ti enrichments near the interface are, however, noted (Fig. 6d, e).

In Palco/C–C couple (Fig. 7a), the droplet was partially debonded from the composite near its contact perimeter (Fig. 7b) although the joint area near the droplet center was sound (Fig. 7c). Some infiltration and reaction of the fibers by braze also was noted (Fig. 7d). In Cusil-ABA/SiC–SiC couple (Fig. 8a), there was partial droplet/composite de-cohesion near the droplet contact perimeter (Fig. 8b)

but there was no delamination within the composite substrate. Most of the droplet/composite contact region near the center was crack-free (Fig. 8c), and exhibited intimate contact between the slurry-cast outer SiC layer on the composite and braze. Interfacial excess of Ti was observed (Fig. 8d) as for the other couples. The contacting SiC fibers were infiltrated and partially covered by braze which solidified during post-braze cooling (Figs. 8e–g). Usually, SiC fibers cracked (Fig. 8g) in a transverse direction (i.e., diametrically) at the boundary between wetted and non-wetted regions. Such cracks could be caused by mechanical stresses from the architecture of the composite (fiber restraints) as well as thermal stresses during joining and solidification.

The measured contact angle (46 – 50° , Table 2) of Palco on C–C appears to be inconsistent with the image of the solidified droplet (Fig. 7a) where the angle on the left side appears to be acute ($<90^\circ$) and the angle on the right side, obtuse ($>90^\circ$). As contact angles were extracted from the spreading behavior of molten droplet, the role of post-cooling shrinkage stresses must be taken into consideration when examining the microstructure of solidified droplets. Figure 7 shows that the solidified droplet has debonded from the heterogeneous C–C substrate. Unlike

Fig. 11 Palco/SiC–SiC couple (#1418, CH, 1,392 K, 5 min): **a** droplet periphery showing an edge crack and separation and flotation of fibers (region ‘A’); **b, c** composite/braze interface for the regions marked ‘A’ and ‘B’ in **a**; and **d, e** composition profiles in regions ‘A’ and ‘B’ of **b** and **c**, respectively



well-polished homogeneous substrates, the residual stress effects may cause anisotropic (non-uniform) shrinkage of the solidifying droplet on heterogeneous C–C surface at which fiber-ply orientations vary. That angles on the two sides of the droplet in Fig. 7a could differ due to solid’s deformation rather than wettability effects is lent credence by the fact that of all brazes examined in the study, Palco has the highest ductility (43%, Table 1).

The Ticusil/SiC–SiC couple (Fig. 9) exhibited droplet/composite de-cohesion (Fig. 9b) as well as delamination within the composite (Fig. 9a, b) near the contact perimeter of the droplet. The contact region near the droplet center exhibited sound metallurgical bonding with the composite (Fig. 9c, d). Titanium enrichments were detected at the

braze/slurry-cast surface layer on the composite as well as at the slurry-cast layer/SiC fiber interface (Fig. 9e, f). There is also possibility of AgCuTi liquid braze infiltrating the contacting fiber tows of SiC–SiC composite via open pores and micro-cracks in the slurry-coated SiC layer on the composite’s surface. The Ti in liquid braze would then react with the SiC coating and form brittle carbides and silicides. The matrix structure within the droplet near the interface exhibits dark plate-like particles which are a Cu–Ti phase and massive gray precipitates, which are a Ti–Si phase (Fig. 10a–c). The Ti enrichments observed at the interface presumably reflect the formation of a TiC layer (a very stable carbide) which is not thick enough to be observed by optical microscopy and conventional SEM. It

Fig. 12 Palni/SiC–SiC couple (#1416, CH, 1,315 K, 5 min): **a** view of the droplet near its contact perimeter showing delamination of fiber plies; **b** flotation of SiC fibers disengaged from the composite; **c, d** higher magnification views of floated fibers, and **e** shows the Si, Ni, and Pd concentrations at point markers in **d**

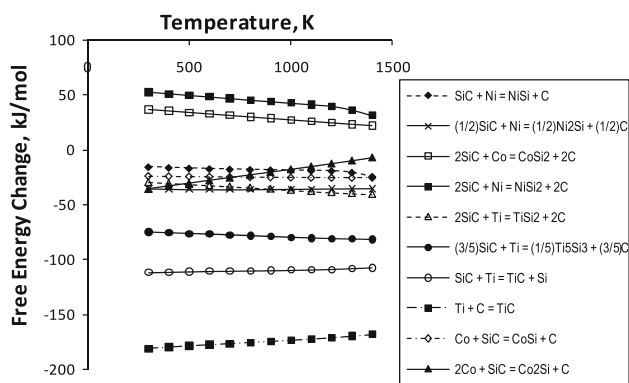
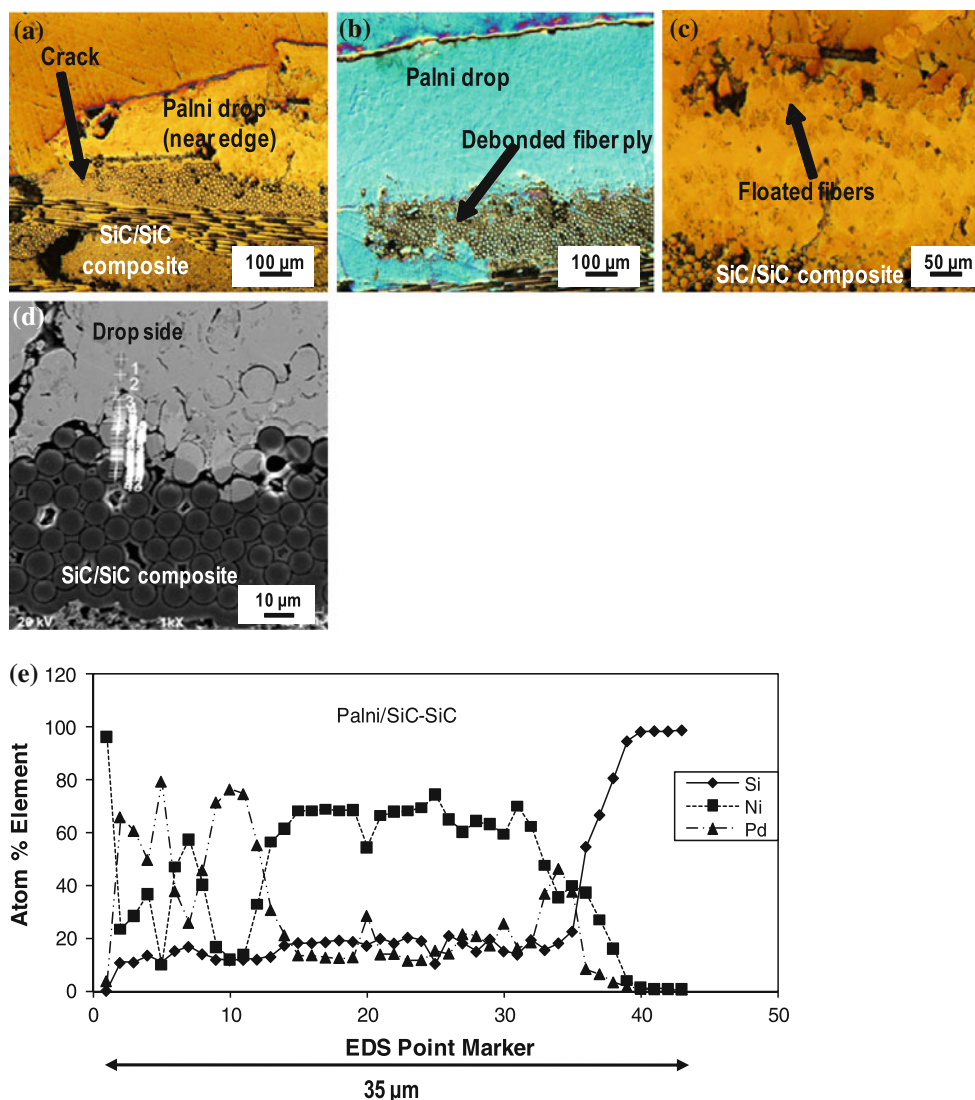


Fig. 13 Free energy change (ΔG) as a function of temperature for reaction between SiC or C and braze constituents Ni, Ti, and Co

has been reported [25] that after a few minutes at 830 °C, a 100 nm thick TiC layer formed at CuAgTi/vitreous carbon interface and led to low (10°–30°) contact angles for this couple.

In both Palco/SiC–SiC (Fig. 11) and Palni/SiC–SiC (Fig. 12) couples, interfacial decohesion between the composite and the droplet had occurred. Additionally, several SiC fiber tows were disengaged from the main body of the SiC–SiC composite, and the separated fibers floated and segregated in the molten droplet (density of Palco and Palni: $10,400 \text{ kg m}^{-3}$) (Figs. 11a, b, 12a–c). Some delamination was observed between the wetted and the non-wetted regions of the composite (e.g., Figs. 11a, 12a). The presence of Co (from Palco) in the composite is observed in Fig. 11d, e. EDS scans along the length of a partially wetted SiC fiber segment (Fig. 11c) show a sharp discontinuity in the elemental Si, Pd, and Co concentrations between the wetted and non-wetted regions. Possible formation of silicides of Pd and Co may have occurred in the wetted region. Likewise, in Palni/SiC–SiC couple (Fig. 12), large Ni concentrations (and relatively modest Pd concentrations) were detected at the boundary between the wetted and non-wetted fibers (Fig. 12d), which points

toward a greater affinity between SiC and Ni than between SiC and Pd.

Joint formation is promoted by the reactions, which yield low contact angles on the substrate. Interactions of C (from C–C composite) with Ti (from Cusil-ABA and Ticusil) could form titanium carbides whereas interactions of SiC (from SiC–SiC composite) with Ni (from Palni) and Co (from Palco) could form silicides of Ni and Co during cooling and solidification. Standard free energy changes (per mole of the metallic species) of several reactions were calculated as a function of temperature using the software HSC Chemistry version 4.1 (Outokumpu Ra, Oy, Finland), and are displayed in Fig. 13. These calculations indicate that whereas NiSi_2 and CoSi_2 are unlikely to form, the phases NiSi, Ni_2Si , TiSi_2 , Ti_5Si_3 , TiC, and CoSi could form ($\Delta G < 0$) during brazing. Only dissolution of SiC into the liquid metal and, eventually, precipitation of graphite (depending on the time of contact between the metal and SiC) are expected at the brazing temperature (silicides would precipitate out during cooling).

As discussed in a preceding paragraph, delamination within the composite was observed near the interface in SiC–SiC joints with Ticusil, Palco, and Palni. Delamination of the SiC–SiC composite was not observed with lowest yield strength (271 MPa, Table 1) Cusil-ABA braze even though shrinkage stresses during cooling caused partial de-cohesion at the interface between the droplet and the composite substrate. A similar behavior was noted for the Palco/C–C couple (Fig. 7) where partial droplet/composite de-cohesion had occurred without delamination within the composite. Palco has a higher ductility (43% elongation) and lower yield strength (341 MPa) than Palni (23% elongation, Y.S.: 772 MPa) and this could lead to relatively less effective accommodation of residual stresses by Palni than Palco.

The mismatch of the coefficient of thermal expansion (CTE) could induce large thermal strains, $\Delta\alpha\Delta T$ ($\Delta\alpha$ —CTE mismatch, ΔT —temperature interval) in the composite substrate. The elastic strains could lead to inter-laminar shear failure of the composite substrate. Representative CTE values for SiC–SiC composite and Cusil-ABA (and Ticusil) are 1.7 to $4.4 \times 10^{-6} \text{ K}^{-1}$ and $18.5 \times 10^{-6} \text{ K}^{-1}$, respectively. For a temperature excursion (ΔT) during brazing of 900°C , the thermal strain would be in the range of ~ 0.0127 – 0.0151 . With the average value of the elastic modulus of SiC–SiC composites as 246 GPa the preceding thermal strains could induce a residual stress of 3.1–3.7 GPa, which exceeds the strength (300–699 MPa) of typical SiC–SiC composites. For the other two brazes, Palco and Palni, the CTE values are not quoted by the manufacturer but theoretical estimates [26] suggest a value of $\sim 15.0 \times 10^{-6} \text{ K}^{-1}$. With a temperature drop for Palco of $1,212^\circ\text{C}$ (higher for Palni) during post-braze cooling,

the thermal strains would be on the order of ~ 0.0122 – 0.0155 , close to the values for joints made using the higher CTE (but lower yield strength) brazes Cusil-ABA and Ticusil. It is conceivable that the relatively low yield strength (Table 1) and good ductility of AgCuTi brazes would permit better stress accommodation than the high yield strength Palco (341 MPa) and Palni (772 MPa) brazes. This conjecture is consistent with the observed composite delamination near the interface in SiC–SiC joints with Ticusil, Palco, and Palni, and the absence of delamination of the SiC–SiC composite in the case of the lowest yield strength (271 MPa, Table 1) braze, Cusil-ABA. However, edge de-cohesion between the droplet and the composite substrate due to shrinkage stresses during post-braze cooling had occurred in the couple.

Conclusions

The spreading behavior and interface microstructure of C–C and SiC–SiC composites in contact with two AgCuTi active brazes and two Pd-base brazes were studied. Sessile drop wettability tests (10^{-6} – 10^{-5} mbar vacuum, 5 min contact) were conducted on unpolished composite substrates using two Pd-base brazes (Pd-40Ni and Pd-35Co), and two AgCuTi brazes (Cusil-ABA and Ticusil). Molten droplets revealed strong anisotropy of spreading because of roughness and chemical inhomogeneity of the composite substrates. Capillary penetration of molten braze occurred within the composites with the C–C composite exhibiting copious penetration by Cusil-ABA and Ticusil. Titanium enrichment at the interface, dissolution of Si (from SiC) in braze and presence of Co (from Palco) in the composite were observed. The contact region at the droplet center exhibited sound metallurgical bonding in all couples except Palni/C–C which failed under low mechanical load. Some inter-laminar shear cracking within the SiC–SiC composites with Ticusil, Palco, and Palni (but not with Cusil-ABA) occurred together with droplet de-cohesion near the joint periphery because of the CTE-mismatch induced stresses during post-braze cooling.

Acknowledgement R. Asthana thankfully acknowledges the research support received from the NASA Glenn Research Center, Cleveland, OH.

References

1. Muolo ML, Ferrera E, Morbelli L, Passerone A (2004) *Scr Mater* 50:325
2. Xiong JT, Li JL, Zhang FS, Huang WD (2006) *Scr Mater* 55:151
3. Blugan G, Kuebler J, Bissig V, Janczak-Rusch J (2007) *Ceram Int* 33(6):1033
4. Ferraris M, Badini C, Montorsi M, Appendino P, Scholz HW (1994) *J Nucl Mater* 212–215(2):1613

5. Asthana R, Singh M (2009) *Scr Mater* 61(3):257
6. Singh M, Asthana R (2009) *Int J Appl Ceram Technol* 6(2):113
7. Singh M, Asthana R (2007) *Mater Sci Eng A* 460:153
8. Singh M, Asthana R (2008) *Compos Sci Technol* 68(14):3010
9. Singh M, Morscher GN, Shpargel TP, Asthana R (2008) *Mater Sci Eng A* 498(1–2):31
10. Singh M, Asthana R, Shpargel TP (2007) *Mater Sci Eng A* 452:699
11. Morscher GN, Singh M, Shpargel TP, Asthana R (2006) *Mater Sci Eng A* 418(1–2):19
12. Singh M, Shpargel TP, Morscher GN, Asthana R (2005) *Mater Sci Eng A* 412:123
13. Singh M, Asthana R, Shpargel TP (2008) *Mater Sci Eng A* 498(1–2):19
14. Klein R, Desmaison-Bruta M, Gineta P, Bellosi A, Desmaison J (2005) *J Eur Ceram Soc* 25:1757
15. Mattia D, Desmaison-Brut M, T'etard D, Desmaison J (2005) *J Eur Ceram Soc* 25:1797
16. Sobczak N, Nogi K, Fujii H, Matsumoto T, Tamaga K, Asthana R (2002) Joining of advanced and specialty materials (JASM-VI). In: Indacochea JE et al (eds) American society for materials. Materials Park, OH
17. Grigorenko N, Poluyanskaya V, Eustathopoulos N, Naidich YV (1998) In: Eustathopoulos N, Sobczak N (eds) Proc. high temperature capillarity. Foundry Research Institute, Krakow, Poland
18. Nogi K, Ogino K (1988) *Trans Jpn Inst Metals* 29(9):742
19. Nikolopoulos P, Agathopoulos S, Angelopoulos GN (1992) *J Mater Sci* 27(1):139. doi: [10.1007/BF00553849](https://doi.org/10.1007/BF00553849)
20. Li SJ, Zhou Y, Duan HP (2002) *J Mater Sci* 37(12):2575. doi: [10.1023/A:1015416312807](https://doi.org/10.1023/A:1015416312807)
21. Hitchcock SJ, Carroll NT, Nicholas MG (1981) *J Mater Sci* 16:714. doi: [10.1007/BF00552210](https://doi.org/10.1007/BF00552210)
22. Eustathopoulos N, Sobczak N, Passerone A, Nogi K (2005) *J Mater Sci* 40(9–10):2271. doi: [10.1007/s10853-005-1945-4](https://doi.org/10.1007/s10853-005-1945-4)
23. Sobczak N, Singh M, Asthana R (2005) *Curr Opin Solid State Mater Sci* 9(4–5):241
24. Nicholas MG, Petevs SD (1994) In: Eustathopoulos N (ed) Proc. high-temperature capillarity (HTC). Slovak Academy of Sciences, Slovakia, p 18
25. Ljungbeg L, Dezellus O, Jeymond M, Eustathopoulos N (1999) In: Vincenzini P (ed) 9th World ceramics congress, ceramics: getting into the 2000's, Part C. Techna Srl, Faenza, p 1011
26. Singh M, Asthana R (2008) In: Krenkel W (ed) Fiber-reinforced ceramic composites. Wiley-VCH, Weinheim, pp 303–325